Nonlinear Dynamics and Systems Theory, **16** (4) (2016) 372–397

New State Space Modelling Approach and Unknown Input Observer Design for the Assessment of Temperature Polarization Phenomenon in Direct Contact Membrane Distillation

M. Chakir *, B. Khoukhi, M. Tadjine and Ms. Boucherit

Process Control Laboratory, Control Engineering Department
Ecole Nationale polytechnique, 10 Avenue Pasteur, Hassan-Badi, Algiers - Algeria

Received: June 19, 2016; Revised: October 10, 2016

Abstract: The objective of this paper is three fold. Firstly, a new modeling approach for direct contact membrane distillation (DCMD) is developed. Based on dynamic bi-dimensional configuration, an uncertain non linear state space model that takes into account all the uncertainties generated by discretization errors and plant parameters variation is derived. It is worth noticing that most of the MD configuration processes have been modeled as steady-state one-dimensional systems. Stationary two-dimensional MD models have been considered only in very few studies. The obtained bi-dimensional state space model of DCMD process is also implemented using Matlab and compared with data published in the literature. Secondly, it is theoretically demonstrated that, by measuring only the inlet and outlet temperatures of the DCMD process, one can recover the temperature profile inside the DCMD process using observers. This is an important point, since most of the existing literatures compute the temperature profile by empirical methods without taking into account disceretization errors and uncertainties. Thirdly, a new unknown input observer is developed to estimate temperature polarization inside the membrane. The convergence of the temperature estimation error to zero is theoretically proved and verified by simulation. Of particular interest, the designed observer can be used for the assessment of temperature polarization phenomena and hence preventing some fouling problems.

Keywords: *direct contact membrane distillation; dynamic modeling; heat and mass transfer; unknown input observer; polarization coefficient; fouling.*

Mathematics Subject Classification (2010): 35Q35, 35Q79, 93A30, 93B07, 93C10, 93C20, 93D30.

* Corresponding author: mailto:chakir_messaoud@yahoo.com

1 Introduction

Membrane distillation (MD) process is an emerging technology for water treatment. The driving force of the MD process results from the pressure difference of vapor formed by a difference in solution's temperature on both sides of a hydrophobic membrane [1]. The advantages of DCMD lie in its simplicity, the need of only small temperature differences and nearly 100% rejection of dissolved solids [1]. Furthermore, thanks to their low energy demand, DCMD processes can be equipped with renewable energy equipment such as solar collectors [2] and solar distillers [3].

Most of researches on DCMD focus on modeling the heat and mass transfer phenomenon inside the membrane, and most of the MD configuration processes have been modeled as steady-state one-dimensional systems using empirical heat and mass transfer equations [4]. Only few publications use stationary one or two-dimensional heat-transfer equation to simulate a particular configuration more accurately. Although many semi-empirical models have been developed, a detailed model for temperature polarization on flat-plate MD processes is still lacking. [5]. In [4] theoretical modeling and experimental analysis of direct contact membrane distillation has been done in steady-state. In [6] a dynamic modeling of direct contact membrane distillation processes has been presented. In [7] performance investigation of a solar-assisted direct contact membrane distillation system is conducted.

This paper presents a different approach using a new bi-dimensional dynamic model to predict the membrane temperature and the pure water flux. It proposes to derive an uncertain state model based on the finite element approximation of the temperature partial differential equations (PDE) and then to build an observer to estimate all temperatures and temperature dependant parameters inside the process from the only measurable data which are inlet and outlet temperatures.

Because temperature distribution inside the membrane is not accessible for measurement this observer is very useful and can be considered as a software sensor to estimate it. The observer developed in this paper is designed in a cascade structure and is specific to the presented DCMD model. It is useful as a means to monitor inner temperature evolution in order to prevent and avoid severe or irreversible fouling situations by predicting their occurrence with a good timing and launching the predefined appropriate maintenance routine [8].

The paper is organized as follows: in the next section, the theoretical equations describing heat and mass transfer in DCMD are introduced and followed by a brief description of fouling phenomenon and its effect on polarization coefficient. In Section 3, a new bi-dimensional state model for DCMD process is developed and simulated. After that, the observability of the whole set of internal dynamic variables is demonstrated, and the new unknown input observer that predicts inner temperature profiles is presented in Section 4. Simulations are conducted to show the efficiency of the proposed observer.

2 DCMD Theoretical Modeling

In Direct Contact Membrane Distillation (DCMD) both sides of the membrane are in direct contact with a liquid stream. On the upper side of the membrane shown in Figure 1 the hot liquid (i.e. hot seawater) flows in the evaporator channel, whilst on the bottom side, a cold liquid (i.e. cooled permeate or distillate) is circulated. Heat and mass transfer occurs from the hotter to the colder side. The liquid in the evaporator channel is

constantly refilled and reheated, whilst the volume of the liquid in the permeate channel increases and heats up. One of the main features of DCMD is that the gas gap between the membrane surface and the condensate stream is very narrow and only exists due to the hydrophobic nature of the membrane. This causes the temperature of the membrane surface in contact with the condensate to be very close to that of the condensate stream itself, thus allowing high temperature drops across the membrane, i.e. high driving forces for mass transfer. Conversely, the direct contact configuration causes a relatively high heat loss as the membrane is the only barrier for the transfer of sensible heat [2].

Mathematical equations describing those phenomena are given in the following paragraphs.

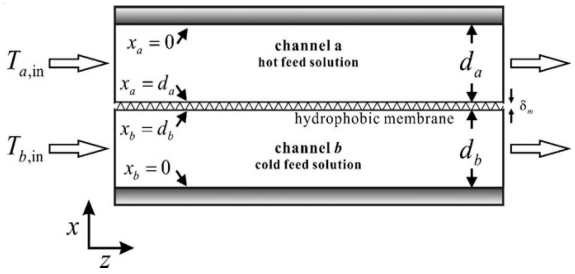

Figure 1: Schematic diagram of DC membrane distillation process [4].

2.1 Mass transfer

The mass transfer driving force across the membrane is the difference in saturated pressure components on both membrane surfaces due to the temperature gradient. The general mass flux form can be expressed as follows:

$$J = c_m \Delta P^{sat} = c_m \left(P_a^{sat} - P_b^{sat} \right), \tag{1}$$

where P_a^{sat}, P_b^{sat} are the saturated pressure of water on the hot and the cold feed membrane surfaces respectively and c_m is the membrane coefficient.

For non-ideal binary mixtures [9], [10], the flux can be determined by:

$$J = c_m \left[(1 - x_{NaCl}) \left(1 - 0.5 x_{NaCl} - 10 x_{NaCl}^2 \right) P_a^{sat} - P_b^{sat} \right], \tag{2}$$

where x_{NaCl} is the mole fraction of $NaCl$ in saline solution.

In the following, the index "s" stands for "side". I.e. $s = a$ for the hot side and $s = b$ for the cold side.

Saturated pressures can be determined by the Antoine equation where T_s is the temperature in $^{\circ}C$, $s = a, b$:

$$P_s^{sat} = 133.32 \times 10^{\left(8.10765 - \left(\frac{1450.286}{T_s + 235}\right)\right)}. \tag{3}$$

The membrane coefficient c_m in (1) can be estimated by a weighted sum via parameters $\alpha(T)$ and $\beta(T)$ of the Knudsen diffusion and the Poiseuille (viscous) flow models [11]:

$$c_m = c_k + c_p,$$

$$c_m = 1.064\ \alpha\left(T\right)\frac{\varepsilon r}{\tau\delta_m}\sqrt{\frac{M_w}{RT_m}} + 0.125\beta\left(T\right)\frac{\varepsilon r^2}{\tau\delta_m}\ \frac{M_w P_m}{\eta_v RT_m}\ , \tag{4}$$

where $\alpha\left(T\right)$ and $\beta\left(T\right)$ are the Knudsen diffusion model and Poiseuille flow model contributions, respectively, M_w is the molecular weight of water, P_m is the mean saturated pressure in membrane, R is the gas constant, r is the pore radius, T_m is the mean temperature in membrane, δ_m is the thickness of membrane, ε is the porosity of membrane, η_v is the gas viscosity and τ is the tortuosity factor. The tortuosity of a porous hydrophobic membrane was estimated by [12].

2.2 Heat transfer

For a laminar and symmetrical flow, symmetrical temperature distribution and without internal energy generation; the temperature propagation in DCMD process is described by the following equation [10]:

$$\rho C_p\left(\frac{\partial T}{\partial t} + \underbrace{u\frac{\partial T}{\partial x} + v\frac{\partial T}{\partial z}}_{convection}\right) = k\left(\underbrace{\frac{\partial^2 T}{\partial x^2} + \frac{\partial^2 T}{\partial z^2}}_{conduction}\right). \tag{5}$$

Considering that conduction effect is along x axis and that convection effect is along z axis, we obtain the basic equation used in DCMD modeling [4]:

$$\rho C_p\left(\frac{\partial T}{\partial t} + v\frac{\partial T}{\partial z}\right) = k\frac{\partial^2 T}{\partial x^2}\ . \tag{6}$$

Velocity along z axis is given by

$$v(x) = 6\overline{v}_s\left(\frac{x}{d_s} - \frac{x^2}{d_s^2}\right), \tag{7}$$

where $\overline{v}_s = \overline{v} = \frac{Q}{d_s W}$ is the mean velocity, Q the volumetric flow, W is the channel width and d_s is its height. Here $d_a = d_b = d$.

We rewrite (5) as follows:

$$\frac{\partial T}{\partial t} = \frac{k}{\rho C_p}\frac{\partial^2 T}{\partial x^2} - v\frac{\partial T}{\partial z} = \alpha\frac{\partial^2 T}{\partial x^2} - v\frac{\partial T}{\partial z}\ , \tag{8}$$

$$\alpha = \frac{k}{\rho C_p}\ . \tag{9}$$

"α" or convective heat transfer coefficient is a time/temperature varying parameter [13] since it depends on thermal conductivity (k), specific heat (C_p) and the density of the seawater (ρ). One can consider variation of α using empirical relations found in specific literature such as those proposed in [4].

2.3 Boundary conditions

The boundary conditions for modelling the DCMD process are given in [4]:

$$\begin{cases} T_s(x,0) = T_{s,in}, \\ \frac{dT_s(0,z)}{dx} = 0, \\ k_a \frac{\partial T_a(d,z)}{\partial x} = -\left[\lambda J + \frac{k_m}{\delta_m}\left(T_a(d,z) - T_b(d,z)\right)\right], \\ k_b \frac{\partial T_b(d,z)}{\partial x} = \left[\lambda J + \frac{k_m}{\delta_m}\left(T_a(d,z) - T_b(d,z)\right)\right]. \end{cases} \tag{10}$$

2.4 Fouling and polarization coefficient in DCMD

2.4.1 Fouling

Fouling in general is the accumulation of unwanted deposits (foulants) on the surface or inside the pores of the membrane that degrade its permeation flux and salt rejection performances (see [8] and references therein such as [14] and [15]). It is one of the major problems in membrane-based processes that reduce the temperature difference across the membrane or increase in temperature polarization leading to lesser driving force [16] (Figure 2).

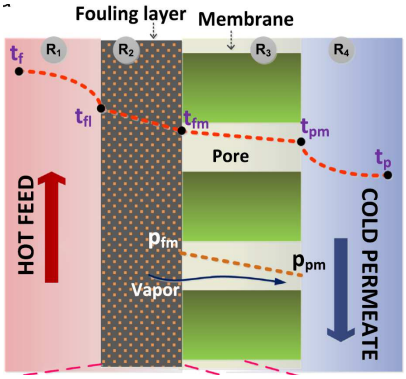

Figure 2: Fouling layer on membrane [8].

The foulants found in membrane technology can be divided into three broad groups according to the fouling material [17]. (a) Inorganic fouling or the deposition of inorganic particles such as calcium carbonate, calcium sulfate, NaCl, ferric oxide, aluminum oxide, etc; (b) organic fouling or the deposition of organic matters such as humic acid, fulvic acid, protein, polysaccharides, and polyacrylic polymers and (c) biological fouling caused by microorganisms such as bacteria and fungi, sludge, algae, yeast, etc. In most cases, a single fouling mechanism does not occur in real MD processes, but a combination of different fouling materials and mechanisms that makes it more complicated to deal with.

Fouling occurs as an external surface fouling referring to the build-up of deposits or gel-like layers on the outer surface of the feed-side of the membrane. Two types of fouling layers are observed [18] both of which decrease the permeate flux: the porous that provides additional heat resistance, thus decreasing the permeate flux and the non-porous deposit layers which reduce the transport of water vapor across the membrane. It also occurs as pore blocking fouling which happens when scales or foulants are formed inside the pores of the membrane causing a partial blocking or gradual narrowing of the pore, or a complete pore blocking (Figure 3) [19].

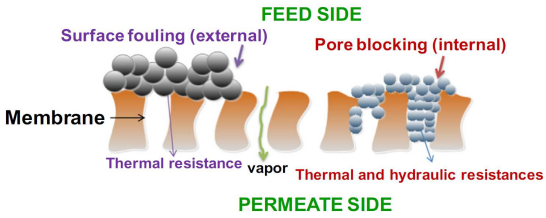

Figure 3: Surface (external) and pore-blocking (internal) fouling [8].

External surface fouling is usually reversible and can be eliminated by chemical cleaning, while internal fouling or pore blocking is in most cases, irreversible leading to damage of the membrane due to compaction of foulants [20].

Fouling is affected by different factors such as [21] (a) foulant characteristics (concentration, molecular size, solubility, diffusivity, hydrophobicity, charge,etc.); (b) membrane properties (hydrophobicity, surface roughness, pore size, surface charge, and surface functional groups); (c) operational conditions (flux, solution temperature, and flow velocity), and (d) feed water characteristics (solution chemistry, pH, ionic strength, and presence of organic/ inorganic matters).

2.4.2 Temperature polarization coefficient

In most MD fouling investigations, membrane fouling is represented by the permeate flux decline [22]. Although membrane fouling is generally interpreted by flux decline, this approach is inadequate for characterizing fouling development in MD, especially due to the effect of temperature in the operation [23] , [24]. Characterizing the foulant on the MD membrane would provide valuable guidance to the effective application of MD operation such as membrane cleaning as well as deciding the necessity for a pretreatment [25]. It is then important to investigate fouling situations taking into account the temperature distribution characteristics such as Temperature Polarization Coefficient (TPC).

The temperatures at the boundary layers of both the feed (hot side) and permeate (cold side) T_{am} and T_{bm} respectively are different from those at the bulk temperatures T_a and T_b due to temperature polarization. Changes in the driving force (i.e., difference in partial water vapor pressure caused by temperature difference) are usually evaluated through TPC given by $TPC = \frac{T_{am}-T_{bm}}{T_a-T_b}$. It indicates the thermal efficiency of the MD system, wherein a value nearing unity suggests good thermal efficiency, and values nearing zero means otherwise [26].

TPC was found to decrease with the decrease of the pore diameter of the fouling layer and also with the decrease of the membrane resistance with respect to the external resistance (see [8] for more information about fouling effects on TPC and methods for fouling monitoring and cleaning).

3 State Space Model Developpement

3.1 Formulation

Since the temperature has a bidimensional space distribution $T = T(x, z)$, we first consider $(M + 1)$ columns separated by constant distance Δz along the z axis with indexes $j = 0, \dots M$ that divide each side of the process into (M) subsystems ${\Sigma^s}_{j=1,..,M}$. In both sides of the process, we consider $(N + 2)$ lines separated by constant distance Δx along the x axis with indexes $i = 0, \dots N + 1$. Let ${}^jT_{s,i}$ be the temperature of the point (i, j) defined by column j and line i in the side s as depicted in Figure 4 bellow.

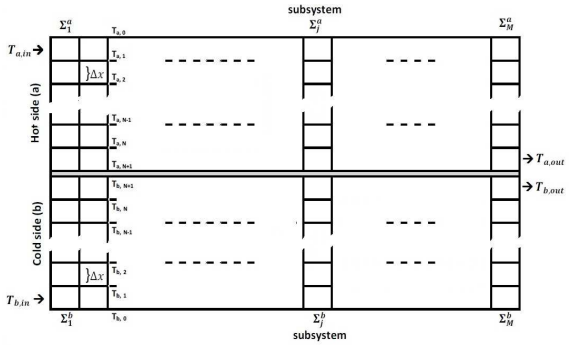

Figure 4: System subdivision.

3.1.1 Derivative terms approximation

Most papers simplify the partial differential equations into an ordinary differential equations system by using the finite difference techniques derived from Taylor's formula with first or second order accuracy [4], [13]

$$\begin{cases} f''(x) = \frac{1}{h^2}\left[f(x+h) - 2f(x) + f(x-h)\right], \\ f'(x) = \frac{1}{h}\left[f(x+h) - f(x)\right] \ or \\ f'(x) = \frac{1}{2h}\left[-3f(x) + 4f(x+h) - f(x+2h)\right], \end{cases} \tag{11}$$

so that for a given point (i, j), conduction term along x axis can be approximated by

$$\frac{\partial^2 \left({}^jT_i\right)}{\partial x^2} = \frac{1}{\Delta x^2}\left({}^jT_{i+1} - 2{}^jT_i + {}^jT_{i-1}\right) \tag{12}$$

and the convection term along z axis by

$$\frac{\partial \left({}^jT_i\right)}{\partial z} = \frac{1}{\Delta z}\left({}^{j+1}T_i - {}^jT_i\right). \tag{13}$$

For our modeling purpose we consider that temperature propagation along z axis is low and can be approximated by a perturbed linear function, therefore we use the following expression for $\frac{\partial\left({}^jT_i\right)}{\partial z}$ where ${}^j\beta_i$ is a bounded perturbation term resulting from modeling approximation

$$\frac{\partial \left({}^jT_i\right)}{\partial z} = \frac{1}{\Delta z}\left({}^jT_i - {}^{j-1}T_i\right) + {}^j\beta_i\ . \tag{14}$$

The velocity profile for the considered point (i, j) is the same for all columns and is given by

$$\begin{cases} v_i = 6\overline{v}\left(\frac{x_i}{d} - \frac{{x_i}^2}{d^2}\right), \\ x_0 = 0,\ x_i = i.\Delta x,\ x_{N+1} = d. \end{cases} \tag{15}$$

Writing (8) for a given point (i, j) in "s" side and substituting ((12),(14)) in it, gives:

$$\frac{\partial\left({}^jT_{s,i}\right)}{\partial t} = {}^j\alpha_{s,i}\ \frac{\partial^2\left({}^jT_{s,i}\right)}{\partial x^2} - v_i\frac{\partial\left({}^jT_{s,i}\right)}{\partial z}, \tag{16}$$

$$\begin{aligned}\frac{\partial\left({}^jT_{s,i}\right)}{\partial t} = \left[{}^j\alpha_{s,i}\ \frac{1}{\Delta x^2}\left({}^jT_{s,i+1} - 2{}^jT_{s,i} + {}^jT_{s,i-1}\right) - \frac{v_{s,i}}{\Delta z}{}^jT_{s,i}\right] + \\ + \frac{v_{s,i}}{\Delta z}{}^{j-1}T_{s,i} + v_{s,i}{}^j\beta_{s,i}\ .\end{aligned} \tag{17}$$

The sign of $\left(v_i{}^j\beta_{s,i}\right)$ does not matter because the perturbation term ${}^j\beta_{s,i}$ is unknown and parameter α for a given subsystem Σ_j^s is (see [4] for $k_{s,i}$, $\rho_{s,i}$ expressions)

$${}^j\alpha_{s,i}\ = \frac{k_{s,i}}{\rho_{s,i}C_{ps}}\ . \tag{18}$$

3.2 Notations and boundary conditions

3.2.1 State variables, output, and input

For a given subsystem Σ_j^s, consider lines with indexes $i = 1, \dots N$ and build a state vector where each state variable reflects the temperature of (i, j) point

$${}^jx_s = \left[{}^jx_{s,1} \dots\ {}^jx_{s,N}\right]^T = \left[{}^jT_{s,1} \dots\ {}^jT_{s,N}\right]^T. \tag{19}$$

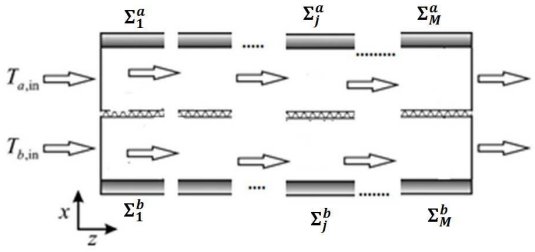

Figure 5: Subsystems in cascade.

Since the flow is laminar one can consider that the output of each subsystem is its own entire state vector. In addition, due to boundary conditions the measurable output temperature of the whole DCMD process given by the last subsystem ($j = M$) is the same at all lines. That means:

$${}^jy_s = {}^jC_s{}^jx_s = {}^jx_s \quad \forall\ j. \tag{20}$$

With the choices made above for ${}^{j}x_s$ and ${}^{j}y_s$, it is easy to see from (17) that the input of each subsystem is the output of the previous one, i. e.

$$ {}^{j}u_s = {}^{j-1}y_s. \tag{21}$$

3.2.2 Boundary conditions

Application of boundary conditions (10) gives:

At the first (resp. last) column: $j = 0$ (resp. $j = M$) that correspond to the first and last inner vertical wall of the DCMD process for both sides, the temperature is the same at all lines and is equal to the inlet (resp. outlet) temperature:

$$\begin{cases} {}^{0}T_{s,i} = T_{s,in} & \forall\ i, \\ {}^{M}T_{s,i} = T_{s,out} & \forall\ i. \end{cases} \tag{22}$$

At the first line $i = 0$ (corresponds to the first inner horizontal wall of the DCMD process)

$$ {}^{j}T_{s,0} = \frac{4^{j}T_{s,1} - {}^{j}T_{s,2}}{3}\ . \tag{23}$$

At the last line $i = N+1$ (corresponds to the boundary layer with the membrane) [4].

For the hot side

$$ {}^{j}T_{a,N+1} = \frac{1}{3}\left[4^{j}T_{a,N} - {}^{j}T_{a,N-1} - \frac{2\Delta x}{k_{a,N}}\left(\lambda J + \frac{k_m}{\delta_m}\left({}^{j}T_{a,N} - {}^{j}T_{b,N}\right)\right)\right]\ . \tag{24}$$

And for the cold side

$$ {}^{j}T_{b,N+1} = \frac{1}{3}\left[4^{j}T_{b,N} - {}^{j}T_{b,N-1} + \frac{2\Delta x}{k_{b,N}}\left(\lambda J + \frac{k_m}{\delta_m}\left({}^{j}T_{a,N} - {}^{j}T_{b,N}\right)\right)\right]\ . \tag{25}$$

3.3 Parameter variation and modelling approximation

Considering for both sides that parameter ${}^{j}\alpha_{s,i}$ has small unknown but bounded variations around a nominal well-known constant value α_{sn} gives (index n means nominal value) :

$$ {}^{j}\alpha_{s,i}\ = \alpha_{sn} + \Delta^{j}\alpha_{s,i}\ , s = \{a, b\}\,, \tag{26}$$

$$\begin{cases} \alpha_{sn} = \frac{k_{an}}{\rho_{sn}C_{ps}}, \\ \left|\Delta^{j}\alpha_{s,i}\ \right| \leqslant \sigma_{\alpha_s}\ \ ;\ \ \sigma_{\alpha_s} > 0. \end{cases} \tag{27}$$

In addition, the bounded perturbation term ${}^{j}\beta_{s,i}$ introduced in (14) is such that:

$$ \left|{}^{j}\beta_{s,i}\right| \leqslant \sigma_{\beta_s}\ \ ;\ \ \sigma_{\beta_s} > 0\ . \tag{28}$$

Then, gathering all variations $\Delta^j\alpha_{s,i}$ in one vector ${}^j\theta_{\alpha s}$ and all perturbation terms ${}^j\beta_{s,i}$ in one vector ${}^j\theta_{\beta s}$ gives :

$$ {}^j\theta_{\alpha s} = \left[{}^j\theta_{\alpha s,1} \dots \ {}^j\theta_{\alpha s,N} \ \right]^T = \left[\Delta^j\alpha_{s,1} \ \dots \ \Delta^j\alpha_{s,N} \ \right]^T, \tag{29} $$

$$ {}^j\theta_{\beta s} = \left[{}^j\theta_{\beta s,1} \dots \ {}^j\theta_{\beta s,N} \ \right]^T = \left[{}^j\beta_{s,1} \dots \ {}^j\beta_{s,N} \ \right]^T. \tag{30} $$

3.4 Equations for state model

The previous states, inputs, and outputs choices, with parameter variation and perturbation terms (17), give a state model of temperature variation at each point (i, j) of the whole process as follows:

$$ \begin{aligned} {}^j\dot{x}_{s,i} = \left[\alpha_{sn} \frac{1}{\Delta x^2} \left({}^jx_{s,i+1} - 2{}^jx_{s,i} + {}^jx_{s,i-1} \right) - \frac{v_{;s,i}}{\Delta z} {}^jx_{s,i} \right] + \frac{v_{s,i}}{\Delta z} {}^ju_{s,i} + \\ + \frac{1}{\Delta x^2} \left({}^jx_{s,i+1} - 2{}^jx_{s,i} + {}^jx_{s,i-1} \right) {}^j\theta_{\alpha s,i} + v_{s,i} {}^j\theta_{\beta s,i} \ . \end{aligned} \tag{31} $$

Equation (31) needs to be detailed for indexes $i = 1$ and $i = N$ in order to include boundary conditions.

For $i = 1$, ${}^jx_{s,0}$ is obtained from (23), and then (31) gives

$$ \begin{aligned} {}^j\dot{x}_{s,1} = \left[\left(-\frac{2}{3}\frac{\alpha_{sn}}{\Delta x^2} - \frac{v_{s,1}}{\Delta z} \right) {}^jx_{s,1} + \frac{2}{3}\frac{\alpha_{sn}}{\Delta x^2} {}^jx_{s,2} \right] + \frac{v_{s,1}}{\Delta z} {}^ju_{s,1} + \\ + \frac{1}{\Delta x^2} \left(-\frac{2}{3} {}^jx_{s,1} + \frac{2}{3} {}^jx_{s,2} \right) {}^j\theta_{\alpha s,1} + v_{s,1} {}^j\theta_{\beta s,1} \ . \end{aligned} \tag{32} $$

For $1 < i < N$, (31) gives:

$$ \begin{aligned} {}^j\dot{x}_{s,i} = \left[\frac{\alpha_{sn}}{\Delta x^2} {}^jx_{s,i-1} - \left(2\frac{\alpha_{sn}}{\Delta x^2} + \frac{v_{s,i}}{\Delta z} \right) {}^jx_{s,i} + \frac{\alpha_{sn}}{\Delta x^2} {}^jx_{s,i+1} \right] + \frac{v_{s,i}}{\Delta z} {}^ju_{s,i} + \\ + \frac{1}{\Delta x^2} \left({}^jx_{s,i-1} - 2{}^jx_{s,i} + {}^jx_{s,i+1} \right) {}^j\theta_{\alpha s,i} + v_{s,i} {}^j\theta_{\beta s,i} \ . \end{aligned} \tag{33} $$

For $i = N$, getting ${}^jx_{a,N+1}$ and ${}^jx_{b,N+1}$ from (24-25) and then considering the following coupling term between Σ_j^a and Σ_j^b

$$ {}^jx_{ab} = 2\Delta x \left(\lambda J + \frac{k_m}{\delta_m} \left({}^jx_{a,N} - {}^jx_{b,N} \right) \right) \tag{34} $$

gives

$$ \left. \begin{aligned} {}^jx_{a,N+1} &= \tfrac{1}{3} \left[4{}^jx_{a,N} - {}^jx_{a,N-1} - \tfrac{{}^jx_{ab}}{k_{a,N}} \right] \\ {}^jx_{b,N+1} &= \tfrac{1}{3} \left[4{}^jx_{b,N} - {}^jx_{b,N-1} + \tfrac{{}^jx_{ab}}{k_{b,N}} \right] \end{aligned} \right\} . \tag{35} $$

This has a compact form as we introduce the variable $\overline{s}$

$$\overline{s} = \frac{2s-a-b}{b-a} = \begin{cases} -1, \ if \ s=a, \\ +1, \ if \ s=b. \end{cases} \tag{36}$$

Equations (35) become:

$$^{j}x_{s,N+1} = \frac{1}{3}\left[4^{j}x_{s,N} - {}^{j}x_{s,N-1} + \overline{s}\frac{^{j}x_{ab}}{k_{s,N}}\right]. \tag{37}$$

Thus (31) gives for $i = N$

$$\begin{aligned} {}^{j}\dot{x}_{s,N} = &\left[\frac{2}{3}\frac{\alpha_{sn}}{\Delta x^2}{}^{j}x_{s,N-1} - \left(\frac{2}{3}\frac{\alpha_{sn}}{\Delta x^2} + \frac{v_{s,i}}{\Delta z}\right){}^{j}x_{s,N}\right] + \frac{v_{s,N}}{\Delta z}{}^{j}u_{s,N} + \\ &+\frac{\alpha_{sn}}{\Delta x^2}\overline{s}\frac{^{j}x_{ab}}{3k_{s,N}} \ + \frac{1}{\Delta x^2}\left(\frac{2}{3}{}^{j}x_{s,N-1} - \frac{2}{3}{}^{j}x_{s,N} + \frac{\overline{s}}{3k_{s,N}}{}^{j}x_{ab}\right){}^{j}\theta_{\alpha s,N} + v_{s,N}{}^{j}\theta_{\beta s,N} \ . \end{aligned} \tag{38}$$

Now, before presenting our first proposition about the new in cascade state model for the DCMD, in particular the state model of a given subsystem Σ_j^s, let us introduce the following matrices, derived from (32), (33) and (38).

- dynamic matrices

$$^{j}A_{s} = \begin{bmatrix} {}^{j}A_{s1} \\ \vdots \\ {}^{j}A_{sN} \end{bmatrix}. \tag{39}$$

The lines of $^{j}A_{s}$ and their elements are

$$\left\{ \begin{array}{c} {}^{j}A_{s1} = [\ a_{s1,1} \ \ a_{s1,2} \ \ 0 \ \ 0 \ldots 0], \\ {}^{j}A_{si} = [0 \ldots 0 \ \ a_{si,i-1} \ \ a_{si,i} \ \ a_{si,i+1} \ 0 \ldots 0], \\ {}^{j}A_{sN} = [0 \ldots 0 \ \ a_{sN,N-1} \ \ a_{sN,N}], \end{array} \right\} \tag{40}$$

$$\left\{ \begin{array}{c} a_{s1,1} = -\left(\frac{2}{3}\frac{\alpha_{sn}}{\Delta x^2} + \frac{v_{s,1}}{\Delta z}\right) \ , \quad a_{s1,2} = \frac{2}{3}\frac{\alpha_{sn}}{\Delta x^2}, \\ a_{si,i-1} = \frac{\alpha_{sn}}{\Delta x^2}, \ a_{si,i} = -\left(2\frac{\alpha_{sn}}{\Delta x^2} + \frac{v_{s,i}}{\Delta z}\right), \ a_{si,i+1} = \frac{\alpha_{sn}}{\Delta x^2}, \\ a_{sN,N-1} = \frac{2}{3}\frac{\alpha_{sn}}{\Delta x^2} \ , \quad a_{sN,N} = -\left(\frac{2}{3}\frac{\alpha_{sn}}{\Delta x^2} + \frac{v_{s,N}}{\Delta z}\right), \end{array} \right\} \tag{41}$$

- input and output matrices

$$\left\{ \begin{array}{c} {}^{j}B_{s} = diag\left({}^{j}B_{si}\right), \ {}^{j}B_{si} = \frac{v_{s,i}}{\Delta z} \ \ \forall \ i, \\ {}^{j}C_{s} = I_{N} \ , \qquad \forall \ j, \end{array} \right\} \tag{42}$$

- perturbation term.

Let ${}^{j}\theta_s$ be the vector of all unknown bounded uncertainties due to parameter variation and modeling approximation and ${}^{j}\Psi_s\left({}^{j}x_s, {}^{j}\theta_s\right)$ be the vector containing all the resulting perturbation terms. It follows:

$$ {}^{j}\theta_s = \left[\begin{array}{c} {}^{j}\theta_{\alpha s} \\ {}^{j}\theta_{\beta s} \end{array} \right], \tag{43} $$

$$ {}^{j}\Psi_s\left({}^{j}x_s, {}^{j}\theta_s\right) = \left[\begin{array}{c} {}^{j}\Psi_{s1} \\ \vdots \\ {}^{j}\Psi_{sN} \end{array} \right]. \tag{44} $$

For $i = 1$

$$ {}^{j}\Psi_{s1} = \frac{1}{\Delta x^2}\left(-\frac{2}{3}{}^{j}x_{s,1} + \frac{2}{3}{}^{j}x_{s,2}\right){}^{j}\theta_{\alpha s,1} + v_{s,1}{}^{j}\theta_{\beta s,1} \ . \tag{45} $$

For $1 < i < N$

$$ {}^{j}\Psi_{si} = \frac{1}{\Delta x^2}\left({}^{j}x_{s,i-1} - 2{}^{j}x_{s,i} + {}^{j}x_{s,i+1}\right){}^{j}\theta_{\alpha s,i} + v_{s,i}{}^{j}\theta_{\beta s,i} \ . \tag{46} $$

For $i = N$:

$$ {}^{j}\Psi_{sN} = \frac{\alpha_{sn}}{\Delta x^2}\overline{s}\frac{{}^{j}x_{ab}}{3k_{s,N}} + \frac{1}{\Delta x^2}\left(\frac{2}{3}{}^{j}x_{s,N-1} - \frac{2}{3}{}^{j}x_{s,N} + \frac{\overline{s}}{3k_{s,N}}{}^{j}x_{ab}\right){}^{j}\theta_{\alpha s,N} + v_{s,N}{}^{j}\theta_{\beta s,N} \ , $$

$$ {}^{j}\Psi_{sN} = \left[\frac{\alpha_{sn}}{\Delta x^2}\overline{s}\frac{{}^{j}x_{ab}}{3k_{s,N}}\frac{1}{{}^{j}\theta_{\alpha s,N}} + \frac{1}{\Delta x^2}\left(\frac{2}{3}{}^{j}x_{s,N-1} - \frac{2}{3}{}^{j}x_{s,N} + \frac{\overline{s}}{3k_{s,N}}{}^{j}x_{ab}\right)\right]{}^{j}\theta_{\alpha s,N} + v_{s,N}{}^{j}\theta_{\beta s,N} \ . \tag{47} $$

A more compact expression of ${}^{j}\Psi_s\left({}^{j}x_s, {}^{j}\theta_s\right)$ would be :

$$ {}^{j}\Psi_s\left({}^{j}x_s, {}^{j}\theta_s\right) = {}^{j}\Psi_{s\alpha}{}^{j}\theta_{\alpha s} + {}^{j}\Psi_{s\beta}{}^{j}\theta_{\beta s} = {}^{j}\Psi_s\left({}^{j}x_S\right){}^{j}\theta_s \tag{48} $$

such that

$$ \left.\begin{array}{c} {}^{j}\Psi_{s\beta} = diag\left({}^{j}\Psi_{s\beta i}\right) \ , \ {}^{j}\Psi_{s\alpha} = diag\left({}^{j}\Psi_{s\alpha i}\right), \\ {}^{j}\Psi_s\left({}^{j}x_S\right) = \left[{}^{j}\Psi_{s\alpha} \ \ {}^{j}\Psi_{s\beta}\right], \end{array}\right\} \tag{49} $$

${}^{j}\Psi_{s\alpha i}$ and ${}^{j}\Psi_{s\beta i}$ are the coefficients of ${}^{j}\theta_{\alpha s,i}$ and ${}^{j}\theta_{\beta s,i}$ in relations (45) to (47) and ${}^{j}\theta_s$ is introduced in (43).

In the following, we give the statement of the uncertain bi-dimensional cascade state model for DCMD process.

Proposition 3.1 *Consider the DCMD process theoretically modeled in Section 2 with the above mentioned matrices and vectors* ${}^{j}A_s$, ${}^{j}B_s$, ${}^{j}C_s$, ${}^{j}x_s$, ${}^{j}u_s$, ${}^{j}y_s$, ${}^{j}\Psi_s$ *and* ${}^{j}\theta_s$. *Then, the inner temperature profile can be predicted using the following set of state space models defined for subsystems* Σ_j^s *(Figure 5)*

$$\Sigma_j^s : \begin{cases} {}^{j}\dot{x}_s = {}^{j}A_s\,{}^{j}x_s + {}^{j}B_s\,{}^{j}u_s + {}^{j}\Psi_s\left({}^{j}x_S\right){}^{j}\theta_s, \\ {}^{j}y_s = {}^{j}C_s\,{}^{j}x_s \qquad j = 1, \dots M. \end{cases} \tag{50}$$

Proof. Direct consequence of the above developments and relations. □

Remark 3.1

- The model is built in cascade as represented in Figure 5 where each subsystem Σ_j^s is supplied by the previous one (Σ_{j-1}^s) and acts on the next one (Σ_{j+1}^s) .
- This form of bi-dimensional state model of DCMD process is introduced for the first time to the best of our knowledge [5] and gives a complete description of the process behavior. It is appropriate for observer based control/monitoring approaches as we will demonstrate in next sections.
- On the basis of this model, we will build an unknown input observer which gives access to suitable information such as polarization ratio and polarization coefficient since it permits to estimate all (i, j) points' temperatures.
- The aim of the work is to give a means to monitor inner temperature evolution in order to prevent and avoid severe or irreversible fouling situations by predicting their occurrence with a good timing and launch the predefined appropriate maintenance routine.
- ${}^{j}\Psi_s\left({}^{j}x_S\right){}^{j}\theta_s$ behaves as a perturbation term and contains errors due to approximation and parameter variation.
- Simulations were conducted to compare model results with some literature data.

3.5 Model simulation

Simulation of the developed state model showed steady state results comparable to [4] using the same data such as geometry, physical properties and operating conditions. The bi-dimensional simulation depicted in Figure 6 shows that temperature in the hot side decreases along x and z axes of the membrane, in the same way the cold side temperature increases along the x and the z axes, which is in agreement with the polarization phenomenon. Figure 7 to Figure 10 show vertical and longitudinal temperature distribution as well as the variation of mass flux densities and velocity effect on pure water production and membrane temperature.

4 Prediction of Temperature Profiles Using Observers

4.1 States and inputs observing

In practice, only the inlet and outlet temperatures are measurable. The profile and longitudinal temperature distributions are not accessible but are very important because they

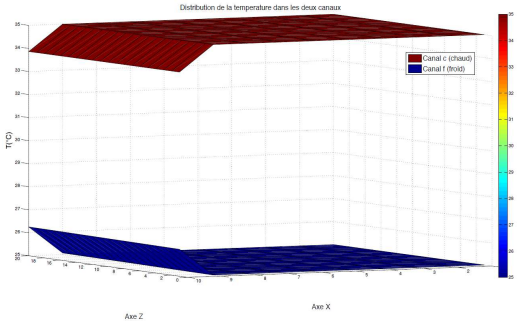

Figure 6: Temperature distribution in two dimensions (up: hot, down: cold).

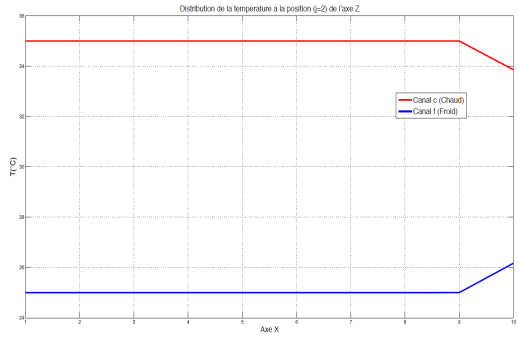

Figure 7: Temperature along x axis for a given z.

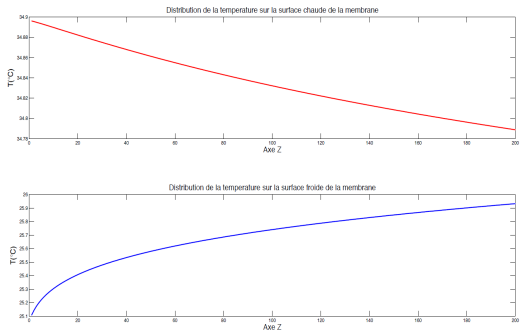

Figure 8: Temperature distribution along the membrane.

describe the polarization phenomenon which is the major driving force for pure water production. The need of an observer arises. The observer should estimate all temperatures inside the process and from those temperatures one could estimate temperature-variable parameters such as polarization coefficient, polarization ratio, and pure water flux.

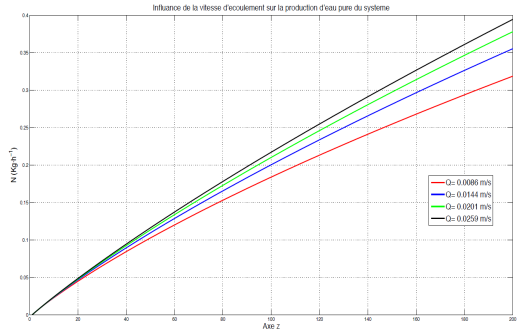

Figure 9: Velocity effect on water production.

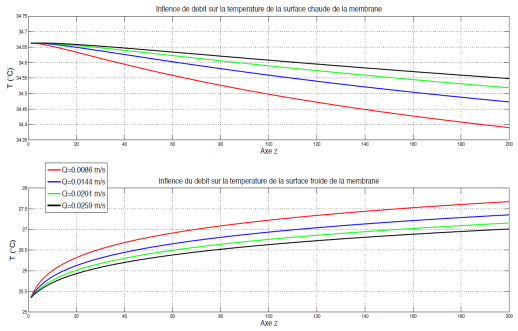

Figure 10: Velocity effect on membrane temperature.

It was stated in Section 3, that the measurable outlet temperature is the same at all lines of the last subsystem Σ_M^s which gives a measurement of the entire output vector. This is due to boundary condition, laminar flow and because generally channel depth (d) is small in DCMD.

On the other hand, outputs, states and inputs have equivalent roles: knowing the state of a subsystem, gives its output and the input of the next one. Conversely, the input informs about the output and the state of the previous one. This motivates the need to build an unknown input observer (UIO) starting from the known (measurable) output of the last subsystem Σ_M^s. The proposed global UIO is built in cascade form (like the state model) as shown bellow in Figure 11 for one side of the process.

The known output ${}^M\hat{y}_s$ (so the state) of the last subsystem Σ_M^s is used with the UIO to estimate its unknown input vector which is the output (and the state) of the previous subsystem Σ_{M-1}^s (${}^M\hat{u}_s = {}^{M-1}\hat{y}_s$). The obtained output (${}^{M-1}\hat{y}_s$) is then used with the UIO to estimate the input of the subsystem Σ_{M-1}^s. This principle is applied to ascend to the first subsystem which has a known input (inlet temperature) and so doing one can have access to all temperatures inside the process.

This structure has a lot of advantages; increasing the accuracy of the model by increasing the number of subsystems; when estimating temperatures inside the process, it is possible to estimate the flux in each part of the membrane, the total flux, and different

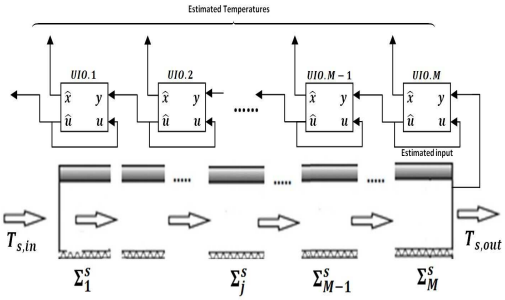

Figure 11: Diagram of the unknown input observer (UIO).

parameters such as polarization ratio and polarization coefficient.

Proposition 4.1 *The states and inputs of models defined in equation (50) are fully observable.*

Proof. Considering the model of Σ_j^s and keeping in mind that for $1 < j < M$, the state vector is the output of the subsystem and the input of the next one, we gather all state vectors in one global vector and write the global unperturbed state model that includes all subsystems. Then, we prove the global state observabilty by showing that global observabilty matrix has a full rank. State and input observablity of each subsystem Σ_j^s follows from the global state observabilty as they are parts of the global state vector.

The unperturbed model of Σ_j^s (without ${}^j\Psi_s\left({}^jx_S\right){}^j\theta_s$) is :

$$\begin{pmatrix} {}^jC_s = I_N \\ {}^ju_s = {}^{j-1}y_s = {}^{j-1}C_s{}^{j-1}x_s = {}^{j-1}x_s \end{pmatrix} \Longrightarrow {}^j\dot{x}_s = {}^jA_s{}^jx_s + {}^jB_s{}^{j-1}x_s \ , \tag{51}$$

which gives for $j = M, \ldots, 1$

$$\begin{cases} {}^M\dot{x}_s = {}^MA_s{}^Mx_s + {}^MB_s{}^{M-1}x_s, \\ \qquad\qquad \vdots \\ {}^1\dot{x}_s = {}^1A_s{}^1x_s + {}^1B_s{}^0x_s, \end{cases} \tag{52}$$

with the compact writing

$$\begin{cases} \dot{X}_g = A_gX_g + B_gU_g, \\ Y_g = C_gX_g, \end{cases} \tag{53}$$

where X_g is the global $[(N \cdot M) \times 1]$ state vector, $U_g = {}^0x_s = {}^1u_s$ and $Y_g = {}^My_s$ are both external measurable input and output temperatures.

$$X_g = \begin{bmatrix} {}^Mx_s{}^T & {}^{M-1}x_s{}^T \ldots {}^1x_s{}^T \end{bmatrix}^T, \ \ U_g = {}^1u_s, \ and \ Y_g = {}^My_s = {}^MC_s{}^Mx_s = {}^Mx_s \ , \tag{54}$$

where A_g is a square $[(N \cdot M) \times (N \cdot M)]$ matrix formed by $(N \times N)$ sized zero matrices except for the main diagonal blocks formed by matrices ${}^jA_s$, $j = M, \ldots, 1$ and upper

next diagonal blocks formed by matrices ${}^{j}B_{s}$, $j = M, \ldots, 2$,

$$\left(\begin{array}{c} A_g = \left[\begin{array}{c} A_{g1} \\ \vdots \\ A_{gM} \end{array} \right], \left\{ \begin{array}{c} A_{g1} = \left[\begin{array}{cccc} \left[{}^{M}A_{s}\right] & \left[{}^{M}B_{s}\right] & [0] \ldots [0] \end{array} \right], \\ A_{gj} = \left[\begin{array}{cccc} [0] \ldots [0] & \left[{}^{j}A_{s}\right] & \left[{}^{j}B_{s}\right] & [0] \ldots [0] \end{array} \right], \\ A_{gM} = \left[\begin{array}{cc} [0] \ldots [0] & \left[{}^{1}A_{s}\right] \end{array} \right], \end{array} \right. \\ - \\ B_g = \left[\begin{array}{c} [0] \\ \vdots \\ [0] \\ \left[{}^{1}B_{s}\right] \end{array} \right], C_g = \left[\begin{array}{cc} \left[{}^{M}C_{s}\right] [0] \ldots [0] \end{array} \right] = \left[\begin{array}{cc} [I_N] [0] \ldots [0] \end{array} \right]. \end{array} \right) \tag{55}$$

Observability matrix is calculated as follows

$$\mathcal{O}(A_g, C_g) = \left[\begin{array}{c} \mathcal{O}_1 \\ \vdots \\ \mathcal{O}_M \end{array} \right] = \left[\begin{array}{c} C_g \\ C_g A_g \\ \vdots \\ C_g A_g^{M-1} \end{array} \right], \tag{56}$$

where $\mathcal{O}(A_g, C_g)$ is triangular due to the particular form of C_g and A_g

$$\left\{ \begin{array}{l} \mathcal{O}_1 = C_g = [[I_N] [0] \ldots \ [0]], \\ \mathcal{O}_2 = C_g A_g = \left[\left[{}^{M}A_{s}\right] \left[{}^{M}B_{s}\right] [0] \ldots \ [0]\right], \\ \mathcal{O}_3 = \mathcal{O}_2 A_g = \left[[\mathcal{O}_{31}] [\mathcal{O}_{32}] \left[{}^{M}{B_s}^{M-1} B_s\right] \ [0] \ldots \ [0]\right], \\ \mathcal{O}_4 = \mathcal{O}_3 A_g = \left[[\mathcal{O}_{41}] [\mathcal{O}_{42}] [\mathcal{O}_{43}] \left[{}^{M}{B_s}^{M-1} {B_s}^{M-2} B_s\right] \ [0] \ldots \ [0]\right], \\ \qquad\qquad \vdots \\ \mathcal{O}_r = [[\mathcal{O}_{r1}] \ldots [\mathcal{O}_{rr-1}] [\mathcal{O}_{rr}] \ [0] \ldots \ [0]], \end{array} \right. \tag{57}$$

with diagonal blocks given by

$$\left\{ \begin{array}{l} \mathcal{O}_{11} = I_N, \\ \mathcal{O}_{rr} = \prod_{k=0}^{k=r-2} {}^{M-k}B_s. \end{array} \right. \tag{58}$$

This yields the simple expression of its determinant

$$|\mathcal{O}(A_g, C_g)| = \prod_{r} |\mathcal{O}_{rr}| . \tag{59}$$

Due to regularity of all ${}^{j}B_{s}$ matrices ($\left|{}^{j}B_{s}\right| \neq 0$) it follows that $\mathcal{O}(A_g, C_g)$ has a full $(N \cdot M)$ rank and thus the global state X_g is fully observable. The state and input of all subsystems Σ_j^s are observable since they are parts of the global state vector. □

4.2 Observer design

The state-models obtained above have the same form for all subsystems in both sides. In order to avoid useless notations, we built the observer (without loss of generality) on

the basis of the following state form where vectors u, x, y and θ and matrices A, B, C and Ψ respectively have the same form and role as in (50)

$$\begin{cases} \dot{x} = Ax + Bu + \Psi(x)\theta, \\ y = Cx. \end{cases} \tag{60}$$

Based on the "known" output of system (60) the design aim is to ensure that observer state and input $(\hat{x}, \hat{u})$ converge to the system state and input (x, u) even with the effect of the unknown perturbation term $\Psi(x)\theta$. We deal with the worst case by considering the maximum possible deviation of θ since we don't need a precise estimation for it.

Proposition 4.2 *Consider the perturbation term $\Psi(x, \theta)$ introduced in (44), and a vector θ_m, such that*

$$\max\left(\|\theta\|, \left\|\hat{\theta}\right\|\right) \leqslant \|\theta_m\| \leqslant \sigma_\theta \ , \tag{61}$$

where $\hat{\theta}$ is the estimate of θ and σ_θ is a positive scalar. Then, Ψ has the following properties:

1) $\Psi(x, \theta)$ is bounded on θ i.e.

$$\begin{cases} \|\Psi(x,\theta)\| \leqslant \|\Psi(x,\theta_m)\| \leqslant \sigma_\theta \|\Psi(x)\|, \\ \left\|\Psi\left(x,\hat{\theta}\right)\right\| \leqslant \|\Psi(x,\theta_m)\| \leqslant \sigma_\theta \|\Psi(x)\|. \end{cases} \tag{62}$$

2) $\Psi(x, \theta)$ is Lipchitz on x i.e.

$$\exists\ \sigma_\Psi > 0 \mid \ \|\Psi(x,\theta) - \Psi(\hat{x},\theta)\| \leqslant \sigma_\Psi \|x - \hat{x}\| \leqslant \sigma_\Psi \tilde{x} \tag{63}$$

and

$$\left\|\Psi(x)\theta - \Psi(\hat{x})\hat{\theta}\right\| = \|\Delta\Psi\| \leqslant \sigma_\Psi \sigma_\theta \tilde{x} \ . \tag{64}$$

Proof. Property 1 results from the multiplicative form of $\Psi(x, \theta)$ given in (48). Properties 2 of Ψ are proved in appendix. □

These properties are used in the following.

Proposition 4.3 *Consider the state space model (60) and the following unknown input observer:*

$$\begin{cases} \dot{\hat{x}} = A\hat{x} + B\hat{u} + \Psi(\hat{x})\hat{\theta} + L(y - \hat{y}), \\ \hat{y} = C\hat{x}, \\ \hat{u} = \eta(y - \hat{y}). \end{cases} \tag{65}$$

Then, estimation errors $\tilde{x} = x - \hat{x}$ and $\tilde{u} = u - \hat{u}$ converge asymptotically to zero if we find symmetric positive-definite matrices P, R and gains η, L with appropriate dimensions that fulfill the following LMI condition:

$$\begin{bmatrix} \left[(A - LC)^T P + P(A - LC) + 2\sigma_\Psi \sigma_\theta P\right] & \left[PB - C^T \eta^T R\right] \\ \left[B^T P - R\eta C\right] & 0 \end{bmatrix} < 0. \tag{66}$$

Proof. State estimation error dynamic is:

$$\dot{\tilde{x}} = (A - LC)\,\tilde{x} + B\tilde{u} + \left(\Psi(x)\,\theta - \Psi(\hat{x})\,\hat{\theta}\right),$$

$$\dot{\tilde{x}} = (A - LC)\tilde{x} + B\tilde{u} + \Delta\Psi\ . \tag{67}$$

Dynamics of u are negligible with respect to $\hat{u}$ due to earlier supposed almost linear temperature propagation along z axis. Thus :

$$\dot{\tilde{u}} = \dot{u} - \dot{\hat{u}} = \dot{u} - \eta C\tilde{x} = -\eta C\tilde{x}\ . \tag{68}$$

Now consider the Lyapunov function ([27], [28]) with symmetric positive-definite matrices P, R:

$$V = \tilde{x}^T P\tilde{x} + \tilde{u}^T R\tilde{u}, \tag{69}$$

$$\begin{gathered}
\dot{V} = \dot{\tilde{x}}^T P\tilde{x} + \tilde{x}^T P\dot{\tilde{x}} + \tilde{u}^T R\dot{\tilde{u}} + \dot{\tilde{u}}^T R\tilde{u}, \\
\dot{V} = \dot{\tilde{x}}^T P\tilde{x} + \tilde{x}^T P\dot{\tilde{x}} - \tilde{u}^T R\eta C\tilde{x} - \tilde{x}^T C^T\eta^T R\tilde{u}, \\
\begin{aligned}
\dot{V} \ &= \tilde{x}^T\left[(A - LC)^T P + P(A - LC)\right]\tilde{x} + \tilde{u}^T B^T P\tilde{x} \\
&+\tilde{x}^T PB\tilde{u} + 2\tilde{x}^T P\Delta\Psi - \tilde{u}^T R\eta C\tilde{x} - \tilde{x}^T C^T\eta^T R\tilde{u}
\end{aligned}, \\
\begin{aligned}
\dot{V} \ &= \tilde{x}^T\left[(A - LC)^T P + P(A - LC)\right]\tilde{x} + \tilde{u}^T\left[B^T P - R\eta C\right]\tilde{x} \\
&+\tilde{x}^T\left[PB - C^T\eta^T R\right]\tilde{u} + 2\tilde{x}^T P\Delta\Psi\ .
\end{aligned}
\end{gathered} \tag{70}$$

From (64):

$$2\tilde{x}^T P\Delta\Psi \le 2\sigma_\Psi\sigma_\theta\tilde{x}^T P\tilde{x}\ . \tag{71}$$

Therefore,

$$\begin{aligned}
\dot{V} \le\ & \tilde{x}^T\left[(A - LC)^T P + P(A - LC) + 2\sigma_\Psi\sigma_\theta P\right]\tilde{x} + \tilde{u}^T\left[B^T P - R\eta C\right]\tilde{x} \\
&+\tilde{x}^T\left[PB - C^T\eta^T R\right]\tilde{u}
\end{aligned} \tag{72}$$

or also $\dot{V} \le [\tilde{x}\ \ \tilde{u}]^T M_V \begin{bmatrix} \tilde{x} \\ \tilde{u} \end{bmatrix}$.

M_V is a matrix given by

$$M_V = \begin{bmatrix} \left[(A - LC)^T P + P(A - LC) + 2\sigma_\Psi\sigma_\theta P\right] & \left[PB - C^T\eta^T R\right] \\ \left[B^T P - R\eta C\right] & 0 \end{bmatrix}. \tag{73}$$

The estimation errors $(\tilde{x}, \tilde{u})$ asymptotically converge to zero if we find matrices η, L, P and R that give a negative-definite $\dot{V}$ ($\dot{V} < 0$). This condition can be announced in the LMI form of Proposition 4.

$$\begin{gathered}
\dot{V} < 0 \Leftrightarrow M_V < 0 \Leftrightarrow \\
\begin{bmatrix} \left[(A - LC)^T P + P(A - LC) + 2\sigma_\Psi\sigma_\theta P\right] & \left[PB - C^T\eta^T R\right] \\ \left[B^T P - R\eta C\right] & 0 \end{bmatrix} < 0\ .
\end{gathered} \tag{74}$$

□

Remark 4.1

- The LMI given in (66) can be solved using the LMI toolbox of MATLAB.
- The proposed observer is similar in spirit the adaptive observers developed in [29], [30], [31], [32].

4.3 Observer simulation

Observer simulation generated a distribution of internal temperatures comparable to those obtained by the model as shown in Figure 12. Figures 13 and 14 show convergence of state estimation errors to zero respectively for hot and cold stream.

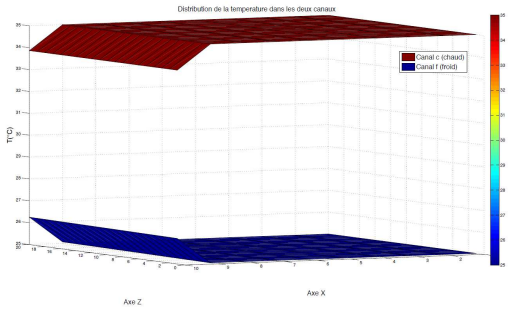

Figure 12: Temperature distribution obtained by the observer.

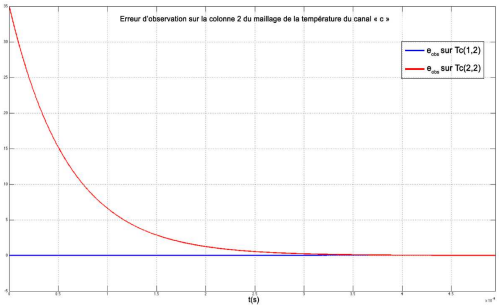

Figure 13: State error convergence in hot side.

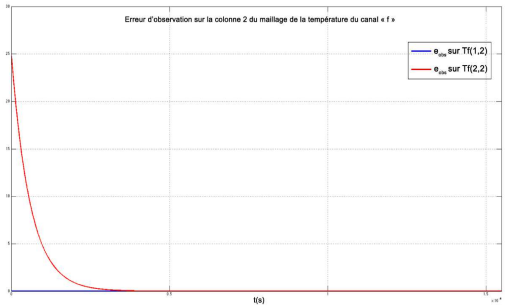

Figure 14: State error convergence in cold side.

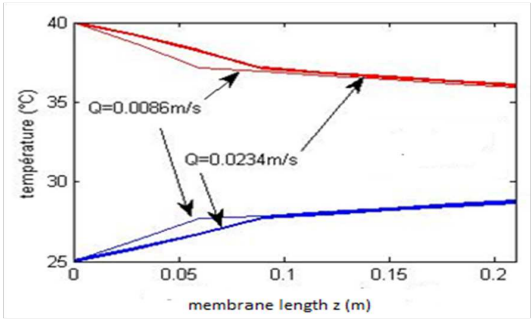

Figure 15: Temperature distribution along z axes.

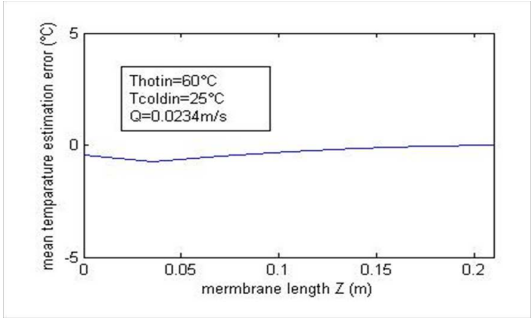

Figure 16: Temperature estimating error along z axes.

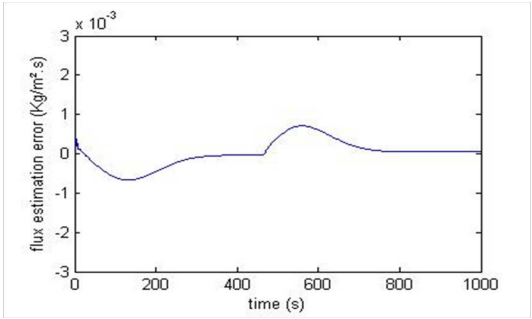

Figure 17: Pure water flux production estimation error.

Other simulations have been made using a different set of parameters for the observer. Figures 15 and 16 show a good estimation of longitudinal temperature distribution compared to those obtained using the model, while Figure 17 shows the ability of the observer to estimate pure water production under varying working conditions (inlet temperature decreases at t=400s) and Figure 18 shows the evolution of temperature polarization coefficient estimating error for a given longitudinal position.

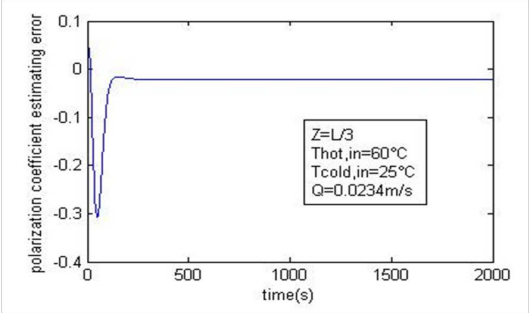

Figure 18: Polarization coefficient estimating error inside DCMD.

Having a good TPC estimation can be very helpful when investigating fouling situations on the basis of pure water decrease information. Thus, the observer-based approach would serve as a means to make further studies about fouling characterization considering in the same time temperature polarization effect on pure water production.

5 Conclusion

In this paper, an observer-based approach is proposed to estimate the temperature profiles inside DCMD unit. This allows predicting the polarization coefficient of the latter and hence can be used to monitor fouling situations. Of particular importance, the convergence of the observation error is proved using Lyapunov direct method and LMI constraints. The performed simulations show the effectiveness of the proposed approach which can be generalized to others types of membrane distillation processes.

Appendix: 2^{nd} Property of $\Psi(x,\theta)$

The objective is to verify that $\Psi(x,\theta)$ is Lipchitz on x i.e.

$$\exists\, \sigma_{\Psi} > 0,\ \|\Psi(x,\theta) - \Psi(\hat{x},\theta)\| \leq \sigma_{\Psi} \|x - \hat{x}\| \leq \sigma_{\Psi} \tilde{x}\ . \tag{75}$$

For more simplicity, relations (43) to (49) describing the vector ${}^{j}\Psi_{s}\left({}^{j}x_{s}, {}^{j}\theta_{s}\right)$ of all perturbation terms, are used without indexes s and j. Therefore, given that Ψ_{β} in (49) does not depend on x, then for the same constant vector $\theta = [\theta_{\alpha}\ \theta_{\beta}\ ]^{T}$, (48) gives:

$$\Psi(x,\theta) - \Psi(\hat{x},\theta) = [\Psi_{\alpha}(x) - \Psi_{\alpha}(\hat{x})]\,\theta_{\alpha}\ . \tag{76}$$

It is then sufficient having (61) to verify that $\Psi_{\alpha}(x)$ is Lipchitz on x

$$\begin{aligned} &\|\Psi(x,\theta) - \Psi(\hat{x},\theta)\| \leq \|\Psi_{\alpha}(x) - \Psi_{\alpha}(\hat{x})\|\,\|\theta_{\alpha}\| \leq \\ &\|\Psi_{\alpha}(x) - \Psi_{\alpha}(\hat{x})\|\,\|\theta_{m}\| \leq \sigma_{\theta}\,\|\Psi_{\alpha}(x) - \Psi_{\alpha}(\hat{x})\|\ . \end{aligned} \tag{77}$$

Consider the vector $\Delta\Psi_{\alpha} = \Psi_{\alpha}(x) - \Psi_{\alpha}(\hat{x}) = [\Delta\Psi_{\alpha,i}]\ ,\ i = 1,\ldots,N$ such that

$$\|\Psi(x) - \Psi(\hat{x})\|^{2} = \|\Delta\Psi_{\alpha}\|^{2} = \sum_{i=1}^{N} (\Delta\Psi_{\alpha,i})^{2} \tag{78}$$

in the following we will make use of this simple property :

$$(p \pm d)^2 \geq 0 \;\Leftrightarrow p^2 + d^2 \geq \mp 2pd \,. \tag{79}$$

We have for $i = 1$

$$\Delta \Psi_{\alpha,1} = \frac{2}{3}\frac{1}{\Delta x^2}\left(-\tilde{x}_1 + \tilde{x}_2\right),$$

$$\left(\Delta \Psi_{\alpha,1}\right)^2 = \frac{4}{9}\frac{1}{\Delta x^4}\left(\tilde{x}_1^2 + \tilde{x}_2^2 - 2\tilde{x}_1\tilde{x}_2\right).$$

Using (79) gives : $-2\tilde{x}_1\tilde{x}_2 \leq \tilde{x}_1^2 + \tilde{x}_2^2$. Then

$$\left(\Delta \Psi_{\alpha,1}\right)^2 \leq \frac{8}{9}\frac{1}{\Delta x^4}\;\left(\tilde{x}_1^2 + \tilde{x}_2^2\right) \leq \frac{1}{\Delta x^4}\;\left(\tilde{x}_1^2 + \tilde{x}_2^2\right)\;. \tag{80}$$

For $1 < i < N$

$$\Delta \Psi_{\alpha,i} = \frac{1}{\Delta x^2}\left(\tilde{x}_{i-1} - 2\tilde{x}_i + \tilde{x}_{i+1}\right),$$

$$\left(\Delta \Psi_{\alpha,i}\right)^2 = \frac{1}{\Delta x^4}\left(\tilde{x}_{i+1}^2 + 4\tilde{x}_i^2 + \tilde{x}_{i-1}^2 - 4\tilde{x}_{i+1}\tilde{x}_i - 4\tilde{x}_i\tilde{x}_{i-1} + 2\tilde{x}_{i+1}\tilde{x}_{i-1}\right)\;.$$

Using (79) gives $2\tilde{x}_{i+1}\tilde{x}_{i-1} \leq \tilde{x}_{i+1}^2 + \tilde{x}_{i-1}^2$, $-4\tilde{x}_{i+1}\tilde{x}_i \leq 4\tilde{x}_{i+1}^2 + \tilde{x}_i^2$, and $-4\tilde{x}_i\tilde{x}_{i-1} \leq 4\tilde{x}_{i-1}^2 + \tilde{x}_i^2$. Thus

$$\left(\Delta \Psi_{\alpha,i}\right)^2 \leq \frac{6}{\Delta x^4}\left(\tilde{x}_{i+1}^2 + \tilde{x}_i^2 + \tilde{x}_{i-1}^2\right)\;. \tag{81}$$

For $i = N$:

$$\Delta \Psi_{\alpha,N} = \frac{1}{\Delta x^2}\left[\frac{2}{3}\left(\tilde{x}_{N-1} - \tilde{x}_N\right) + \left(\frac{\alpha_n}{\theta_{\alpha,N}} + 1\right)\tilde{x}_{ab}\right] \leq \frac{1}{\Delta x^2}\left[\frac{2}{3}\left(\tilde{x}_{N-1} - \tilde{x}_N\right) + \sigma_1\tilde{x}_{ab}\right]\;,$$

where σ_1 is a majoration of $\left(\frac{\alpha_n}{\theta_{\alpha,N}} + 1\right)$ and $\tilde{x}_{ab}$ obtained from (34) verifies :

$\tilde{x}_{ab} \;= \frac{\Delta 2 x k_m}{\delta_m}\left(\tilde{x}_{a,N} - \tilde{x}_{b,N}\right) \Rightarrow \tilde{x}_{ab}^2 = \left(\frac{2\Delta x k_m}{\delta_m}\right)^2\left(\tilde{x}_{a,N} - \tilde{x}_{b,N}\right)^2 \leq \sigma_2\tilde{x}_N^2$ where σ_2 is an appropriate majoration.

It follows:

$$\left(\Delta \Psi_{\alpha,N}\right)^2 \leq \frac{1}{\Delta x^4}\left[\left(\frac{2}{3}\left(\tilde{x}_{N-1} - \tilde{x}_N\right)\right)^2 + 2\frac{2\sigma_1}{3}\tilde{x}_{ab}\left(\tilde{x}_{N-1} - \tilde{x}_N\right) + \sigma_1^2\tilde{x}_{ab}^2\right]. \tag{82}$$

As for $\Delta \Psi_{\alpha,1}$ we obtain $\left(\frac{2}{3}\left(\tilde{x}_{N-1} - \tilde{x}_N\right)\right)^2 \leq \tilde{x}_N^2 + \tilde{x}_{N-1}^2$ and (79) gives: $2\tilde{x}_{ab}\left(\tilde{x}_{N-1} - \tilde{x}_N\right) \leq \tilde{x}_{ab}^2 + \left(\tilde{x}_{N-1} - \tilde{x}_N\right)^2 \leq \sigma_2\tilde{x}_N^2 + 2\tilde{x}_N^2 + 2\tilde{x}_{N-1}^2$.

Gathering the terms and taking $\sigma_N = \left(1 + \sigma_2\frac{2\sigma_1}{3} + 2\frac{2\sigma_1}{3} + \sigma_1^2\sigma_2\right)$, one gets:

$$\left(\Delta \Psi_{\alpha,N}\right)^2 \leq \frac{1}{\Delta x^4}\left[\tilde{x}_N^2\left(1 + \sigma_2\frac{2\sigma_1}{3} + 2\frac{2\sigma_1}{3} + \sigma_1^2\sigma_2\right) + \tilde{x}_{N-1}^2\left(1 + 2\frac{2\sigma_1}{3}\right)\right]$$

$$\left(\Delta \Psi_{\alpha,N}\right)^2 \leq \frac{\sigma_N}{\Delta x^4}\left[\tilde{x}_N^2 + \tilde{x}_{N-1}^2\right]\;. \tag{83}$$

Finally from (80), (81)-(83)

$$\sum_{i=1}^{N}\left(\Delta\Psi_{\alpha,i}\right)^2=\left(\Delta\Psi_{\alpha,1}\right)^2+\sum_{i=2}^{N-1}\left(\Delta\Psi_{\alpha,i}\right)^2+\left(\Delta\Psi_{\alpha,N}\right)^2$$

$$\leq\frac{1}{\Delta x^4}\left[\tilde{x}_1^2+\tilde{x}_2^2+6\sum_{i=2}^{N-1}\left(\tilde{x}_{i+1}^2+\tilde{x}_i^2+\tilde{x}_{i-1}^2\right)\ +\sigma_N\left[\tilde{x}_N^2+\tilde{x}_{N-1}^2\right]\right]$$

$$\leq\frac{\max\left(6,\sigma_N\right)}{\Delta x^4}\left[\tilde{x}_1^2+\tilde{x}_2^2+\sum_{i=3}^{N}\tilde{x}_i^2+\sum_{i=2}^{N-1}\tilde{x}_i^2+\sum_{i=1}^{N-2}\tilde{x}_i^2\ +\tilde{x}_N^2+\tilde{x}_{N-1}^2+\tilde{x}_1^2+\tilde{x}_N^2\right]$$

$$\sum_{i=1}^{N}\left(\Delta\Psi_{\alpha,i}\right)^2\leq\frac{3\max\left(6,\sigma_N\right)}{\Delta x^4}\sum_{i=1}^{N}\tilde{x}_i^2 \tag{84}$$

and

$$\|\Psi_\alpha\left(x\right)-\Psi_\alpha\left(\hat{x}\right)\|\leq\sqrt{\frac{3\max\left(6,\sigma_N\right)}{\Delta x^4}}\sqrt{\sum_{1}^{N}\tilde{x}_i^2}. \tag{85}$$

There exists $\sigma_\Psi>0$ such that

$$\|\Psi\left(x,\theta\right)-\Psi\left(\hat{x},\theta\right)\|\leq\sigma_\Psi\left\|x-\hat{x}\right\|\leq\sigma_\Psi\tilde{x}\ ,$$

i.e. $\Psi\left(x,\theta\right)$ is Lipschitz on x.

From the above inequality and relation (61), one has

$$\left\|\Psi\left(x\right)\theta-\Psi\left(\hat{x}\right)\hat{\theta}\right\|=\left\|\Delta\Psi\right\|\leq\sigma_\Psi\sigma_\theta\tilde{x}\ .$$

□

References

[1] Lawson, K.W. and Lloyd, D.R. Membrane distillation II: Direct contact MD. *Journal of Membrane Science* **120** (1) (1996) 123–133.

[2] Koschikowski, J., Wieghaus, M. and Rommel, M. Solar thermal-driven desalination plants based on membrane distillation. *Desalination* **156** (1-3) (2003) 295–304.

[3] De Andrs, M.C. Doria, J., Khayet, M., Pena, L. and Mengual, J.I. Coupling of a membrane distillation module to a multi effect distiller for pure water production. *Desalination* **115** (1) (1998) 71–81.

[4] Chen, T., Ho, C., and Yeh, H. Theoretical modeling and experimental analysis of direct contact membrane distillation. *Journal of Membrane Science* **330** (1-2) (2009) 279-287.

[5] Hitsov, I., Maere, T., De Sitter, K., Dotremont, C. and Nopens, I. Modelling approaches in membrane distillation: A critical review. *Separation and Purification Technology* **142** (2015) 48–64.

[6] Bin Ashoor, B., Fath, H., Marquardt,W. and Mhamdi, A. Dynamic modeling of direct contact membrane distillation processes. In: *Proceedings of the 11th International Symposium on Process Systems Engineering.* Singapore, 2012, P. 15–19.

[7] Kim, Y.D, Thu, K., Ghaffour, N., and Choon Ng, K. Performance investigation of a solar-assisted direct contact membrane distillation system. *Journal of Membrane Science* **427** (1x) (2013) 345–364.

[8] Tijing, L.D., Woo, Y.C., Choi, J.S., Lee, S., Kim, S.H. and Shon, H.K. Fouling and its control in membrane distillation – A review. *Journal of Membrane Science* **475** (2015) 215–244.

[9] Lawson, K.W. and Lloyd, D.R. Membrane distillation. *Journal of Membrane Science* **124** (1) (1997) 1–25.

[10] Felder, R.M. and Rousseau, R.W. *Elementary Principles of Chemical Processes 3rd ed.* John Wiley & Sons, New York, 2000.

[11] Schofield, R.W., Fane, A.G. and Fell, C.G.D. Gas and vapor transport through microporous membrane. *Journal of Membrane science* **53** (1-2) (1990) 159–171.

[12] Iversen, S.B., Bhatia,V.K., Dam-Jphasen, K. and Jonsson, G. Characterization of microporous membranes for use in membrane contactors. *Journal of Membrane science* **130** (1-2) (1997) 205–217.

[13] Eleiwi, F., Laleg-Kirati, T.M. Dynamic modeling and optimization in membrane distillation system. In: *Preprints of the 19th World Congress, The International Federation of Automatic Control.* Cape Town, South Africa, 2014, 24–29.

[14] Gryta, M. Influence of polypropylene membrane surface porosity on the performance of membrane distillation process. *Journal of Membrane science* **287** (1) (2007) 67–78.

[15] He, F., Gilron, J., Lee, H. Song, L. and Sirkar, K.K. Potential for scaling by sparingly soluble salts in cross flow DCMD. *Journal of Membrane science* **311** (1-2) (2008) 68–80.

[16] Hsu, S.T., Cheng, K.T. and Chiou, J.S. Sea water desalination by direct contact membrane distillation. *Desalination* **143** (3) (2002) 279–287.

[17] Meng, F., Chae, S.R., Drews, A., Kraume, M., Shin, H.-S. and Yang, F. Recent advances in membrane bioreactors (MBRs): Membrane fouling and membrane material. *Water Research* **43** (6) (2009) 1489–1512.

[18] Gryta, M. Fouling in direct contact membrane distillation process. *Journal of Membrane Science* **325** (1) (2008) 383–394.

[19] Knyazkova, T.V. and Maynarovich, A.A. Recognition of membrane fouling: testing of theoretical approaches with data on NF of salt solutions containing a low molecular weight surfactant as a foulant. *Desalination* **126** (1-3) (1999) 163–169.

[20] Hoek, E.M.V., Allred, J., Knoell, T. and Jeong, B.-H. Modeling the effects of fouling on full-scale reverse osmosis processes. *Journal of Membrane science* **314** (1-2) (2008) 33–49.

[21] El-Bourawi, M.S., Ding, Z., Ma, R. and Khayet, M. A frame work for better understanding membrane distillation separation process. *Journal of Membrane Science* **285** (1-2) (2006) 4–29.

[22] Khayet, M., Velzquez A. and Mengual, J.I. Direct contact membrane distillation of humic acid solutions. *Journal of Membrane Science* **240** (1-2) (2004) 123–128.

[23] Srisurichan, S., Jiraratananon, R. and Fane, A.G. Humic acid fouling in the membrane distillation process. *Desalination* **174** (1) (2005) 63–72.

[24] Gryta, M., Tomaszewska, M., Grzechulska, J. and Morawski, A.W. Membrane distillation of NaCl solution containing natural organic matter. *Journal of Membrane Science* **181** (2) (2001) 279–287.

[25] Naidu, G., Jeong, S., Kimb, S.J., Kim, I.S. and Vigneswaran, S. Organic fouling behavior in direct contact membrane distillation. *Desalination* **347** (2014) 230–239.

[26] Martínez-Díez, L. and Vzquez-Gonzlez, M.I. Temperature and concentration polarization in membrane distillation of aqueous salt solutions. *Journal of Membrane Science* **156** (2) (1999) 265–273.

[27] Chekireb,H. Tadjine, M. and Djemaï, M. On a Class of Manifolds for Sliding Mode Control and Observation of Induction Motor. *Nonlinear Dynamics and Systems Theory* **8** (1) (2008) 21–34.

[28] Chekireb,H. Tadjine, M. and Djemaï, M. Lyapunov Based on Cascaded Non-linear Control of Induction Machine. *Nonlinear Dynamics and Systems Theory* **7** (3) (2007) 253–266.

[29] Boulkroune, A., Tadjine, M., M'Saad, M. and Farza,M. How to design a fuzzy adaptive controller based on observers for uncertain affine nonlinear systems. *Fuzzy Sets Syst* **159** (8) (2008) 926–948.

[30] Boulkroune, A., Tadjine, M., M'Saad, M. and Farza,M. Adaptive fuzzy observer for uncertain nonlinear systems. *Control Intell. Syst* **39** (3) (2011) 145–150.

[31] Boulkroune, A., Tadjine, M., M'Saad, M. and Farza,M. Design of a unified adaptive fuzzy observer for uncertain nonlinear systems. *Information Sciences* **265** (2014) 139–153.

[32] Gupta, M. K. Tomar, N. K. and Bhaumik, S. Observer Design for Descriptor Systems with Lipschitz Nonlinearities: an LMI Approach. *Nonlinear Dynamics and Systems Theory* **14** (3) (2014) 292–302.